

AD-A166 159

MICROWAVE EMISSION FROM A NONRELATIVISTIC ELECTRON BEAM 1/1

(U) KAHAN SCIENCES CORP COLORADO SPRINGS CO

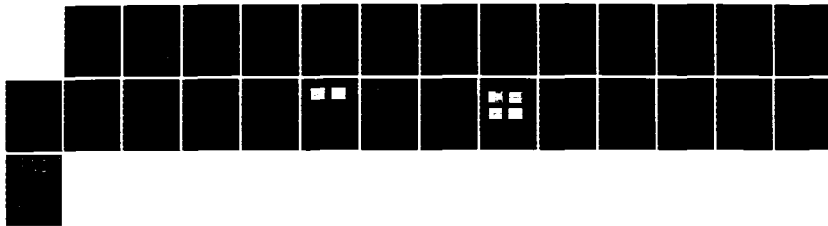
S FACE ET AL. 31 OCT 84 K-85-111U(R) DWA-TR-85-19

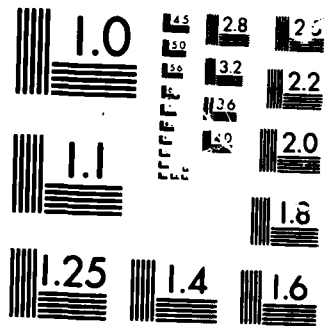
UNCLASSIFIED

DWA001-83-C-0002

F/G 9/5

NL





MICROCOPY RESOLUTION TEST CHART

2

AD-A166 159

DNA-TR-85-19

MICROWAVE EMISSION FROM A NONRELATIVISTIC ELECTRON BEAM

**S. Face W. Hobbs
E. Cozart T. Tumolillo
Kaman Sciences Corporation
1500 Garden of the Gods Road
P. O. Box 7463
Colorado Springs, CO 80933-7463**

31 October 1984

Technical Report

CONTRACT No. DNA 001-83-C-0002

**Approved for public release;
distribution is unlimited.**

THIS WORK WAS SPONSORED BY THE DEFENSE NUCLEAR AGENCY
UNDER RDT&E RMSS CODE B323083466 X99QAXVE00053 H2590D.

**DTIC
ELECTE
APR 11 1986
B**

**Prepared for
Director
DEFENSE NUCLEAR AGENCY
Washington, DC 20305-1000**

DTIC FILE COPY

86 2 7 007

Destroy this report when it is no longer needed. Do not return to sender.

PLEASE NOTIFY THE DEFENSE NUCLEAR AGENCY,
ATTN: STTI, WASHINGTON, DC 20305-1000, IF YOUR
ADDRESS IS INCORRECT, IF YOU WISH IT DELETED
FROM THE DISTRIBUTION LIST, OR IF THE ADDRESSEE
IS NO LONGER EMPLOYED BY YOUR ORGANIZATION.



UNCLASSIFIED

SECURITY CLASSIFICATION OF THIS PAGE

10-11-85

REPORT DOCUMENTATION PAGE				Form Approved OMB No. 0704-0188 Exp. Date. Jun 30, 1986	
1a REPORT SECURITY CLASSIFICATION UNCLASSIFIED			1b RESTRICTIVE MARKINGS		
2a SECURITY CLASSIFICATION AUTHORITY N/A since Unclassified		3 DISTRIBUTION AVAILABILITY OF REPORT Approved for public release; distribution is unlimited.			
2b DECLASSIFICATION/DOWNGRADING SCHEDULE N/A since Unclassified					
4 PERFORMING ORGANIZATION REPORT NUMBER(S) K-85-111U(R)			5 MONITORING ORGANIZATION REPORT NUMBER(S) DNA-TR-85-19		
6a NAME OF PERFORMING ORGANIZATION Kaman Sciences Corporation		6b OFFICE SYMBOL (if applicable)	7a NAME OF MONITORING ORGANIZATION Director Defense Nuclear Agency		
6c ADDRESS (City, State, and ZIP Code) 1500 Garden of the Gods Road P.O. Box 7463 Colorado Springs, CO 80933-7463			7b ADDRESS (City, State, and ZIP Code) Washington, DC 20305-1000		
8a NAME OF FUNDING SPONSORING ORGANIZATION		8b OFFICE SYMBOL (if applicable)	9 PROCUREMENT INSTRUMENT IDENTIFICATION NUMBER DNA 001-83-C-0002		
8c ADDRESS (City, State, and ZIP Code)			10 SOURCE OF FUNDING NUMBERS		
		PROGRAM ELEMENT NO 62715H	PROJECT NO X99QAXV	TASK NO E	WORK UNIT ACCESSION NO DH006520
11 TITLE (Include Security Classification) MICROWAVE EMISSION FROM A NONRELATIVISTIC ELECTRON BEAM					
12 PERSONAL AUTHOR(S) Face, S.; Hobbs, W.; Cozart, E.; Tumolillo, T.					
13a TYPE OF REPORT Technical Report		13b TIME COVERED FROM 840103 TO 841031	14 DATE OF REPORT (Year, Month, Day) 841031		15 PAGE COUNT 28
16 SUPPLEMENTARY NOTATION This work was sponsored by the Defense Nuclear Agency under RDT&E RMSS Code B323083466 X99QAXVE00053 H2590D.					
17 COSATI CODES			18 SUBJECT TERMS (Continue on reverse if necessary and identify by block number)		
FIELD	GROUP	SUB-GROUP	Microwave Emission Microwave Experiment		
20	08		High-Frequency Threat		
16	01		Electron Beam		
19 ABSTRACT (Continue on reverse if necessary and identify by block number)					
<p>Testing was conducted at the Physics International MBS Facility during the time periods of 9-20 July and 4-7 September to investigate the interaction between an ambient plasma and a simulated photoelectron boundary layer. During the test period, 241 shots were taken on the electron-beam generator, resulting in approximately 1,500 data recordings.</p> <p>The primary purpose of the test program was to measure the microwave energy emitted by the electron distribution both with and without the presence of an ambient plasma, presumably due to virtual cathode phenomena or reflexing of the emitted electrons. The peak energy of the electron beam was about 140 keV, and the average current density was in the range of 1 to 7 A/cm² over 730 cm². This translates to an average electron density of approximately 10⁸ to 10⁹ per cubic centimeter. Both discrete and broadband microwave radiation were observed with an ambient plasma of density 10⁸ to 10¹⁰ electrons/cm³. Efficiency for the conversion of electron energy to microwave energy is in the range of 0.05 to 0.03 percent.</p>					
20 DISTRIBUTION AVAILABILITY OF ABSTRACT <input type="checkbox"/> UNCLASSIFIED UNLIMITED <input checked="" type="checkbox"/> SAME AS RPT <input type="checkbox"/> DTIC USERS			21 ABSTRACT SECURITY CLASSIFICATION UNCLASSIFIED		
22a NAME OF RESPONSIBLE PERSONAL Betty L. Fox		22b TELEPHONE (Include Area Code) (202) 325-7042		22c OFFICE SYMBOL DNA/STTI	

DD FORM 1473, 8-78

Use of this form by the user and its contents
 All other editions are obsolete

SECURITY CLASSIFICATION OF THIS PAGE

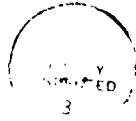
UNCLASSIFIED

SUMMARY

Testing was conducted at the Physics International MBS Facility during the time periods of 9-20 July and 4-7 September to investigate the interaction between an ambient plasma and a simulated photoelectron boundary layer. During the test period, 241 shots were taken on the electron-beam generator, resulting in approximately 1,500 data recordings.

The primary purpose of the test program was to measure the microwave energy emitted by the electron distribution both with and without the presence of an ambient plasma. A microwave spectrometer covering the frequency range 1.12 to 18 GHz was used. Broadband microwave radiation was observed in the absence of an ambient plasma, presumably due to virtual cathode phenomena or reflexing of the emitted electrons. The peak energy of the electron beam was about 140 keV, and the average current density was in the range of 1 to 7 A/cm² over 730 cm². This translates to an average electron density of approximately 10⁸ to 10⁹ per cubic centimeter. Both discrete and broadband microwave radiation were observed with an ambient plasma of density 10⁸ to 10¹⁰ electrons/cm³. Efficiency for the conversion of electron energy to microwave energy is in the range of 0.05 to 0.3 percent.

Accession No. _____
NTIS _____ ✓
GPO _____
Contract _____
Author _____
Title _____
Distrib _____
Av _____
Dist _____
A-1



Conversion factors for U.S. Customary to metric (SI) units of measurement.



angstrom	1 000 000 X E -10	meters (m)
atmosphere (normal)	1 013 25 X E +2	kilo pascal (kPa)
bar	1 000 000 X E +2	kilo pascal (kPa)
barn	1 000 000 X E -28	meter ² (m ²)
British thermal unit (thermochemical)	1 054 350 X E +3	joule (J)
calorie (thermochemical)	4 184 000	joule (J)
cal (thermochemical)/cm ²	4 184 000 X E -2	mega joule/m ² (MJ/m ²)
curie	3 700 000 X E +1	*giga becquerel (GBq)
degree (angle)	1 745 329 X E -2	radian (rad)
degree Fahrenheit	$t_c = (t_f + 459.67)/1.8$	degree kelvin (K)
electron volt	1 602 19 X E -19	joule (J)
erg	1 000 000 X E -7	joule (J)
erg/second	1 000 000 X E -7	watt (W)
foot	3 048 000 X E -1	meter (m)
foot-pound-force	1 355 818	joule (J)
gallon (U.S. liquid)	3 785 412 X E -3	meter ³ (m ³)
inch	2 540 000 X E -2	meter (m)
jerk	1 000 000 X E +9	joule (J)
joule/kilogram (J/kg) (radiation dose absorbed)	1 000 000	Gray (Gy)
kilotons	4 183	terajoules
kip (1000 lbf)	4 448 222 X E +3	newton (N)
kip/inch ² (ksi)	6 894 757 X E +3	kilo pascal (kPa)
ktap	1 000 000 X E +2	newton-second/m ² (N-s/m ²)
micron	1 000 000 X E -6	meter (m)
mil	2 540 000 X E -5	meter (m)
mile (international)	1 609 344 X E -3	meter (m)
ounce	2 834 952 X E -2	kilogram (kg)
pound-force (lbs avoirdupois)	4 448 222	newton (N)
pound-force/inch	1 129 848 X E -1	newton-meter (N.m)
pound-force/inch	1 751 268 X E +2	newton/meter (N/m)
pound-force/foot ²	4 798 026 X E -2	kilo pascal (kPa)
pound-force/inch ² (psi)	6 894 757	newton-meter (N.m)
pound-mass (lbm avoirdupois)	4 535 924 X E -1	kilogram (kg)
pound-mass-foot ² (moment of inertia)	4 214 011 X E -2	kilogram-meter ² (kg·m ²)
pound-mass/foot ³	1 601 846 X E +1	kilogram/meter ³ (kg/m ³)
rad (radiation dose absorbed)	1 000 000 X E -2	*Gray (Gy)
roentgen	2 579 760 X E -4	coulomb/kilogram (C/kg)
shake	1 000 000 X E -8	second (s)
slug	1 459 390 X E +1	kilogram (kg)
torr (mm Hg, 0°C)	1 333 22 X E -1	kilo pascal (kPa)

*The becquerel (Bq) is the SI unit of radioactivity; 1 Bq = 1 event/s.
 **The Gray (Gy) is the SI unit of absorbed radiation.

A more complete listing of conversions may be found in "Metric Practice Guide E 380-74," American Society for Testing and Materials

TABLE OF CONTENTS

Section		Page
	SUMMARY	iii
	CONVERSION TABLE	iv
	LIST OF ILLUSTRATIONS	vi
	LIST OF TABLES	vi
1	TEST CONFIGURATION	1
2	DIAGNOSTIC EQUIPMENT	2
	2.1 Microwave	2
	2.2 Electron Beam	4
	2.3 Ambient Plasma	4
3	TEST MATRIX	5
4	TEST RESULTS	6
	4.1 Calibration Measurements	6
	4.2 Plasma Measurements	6
5	RECOMMENDATIONS	15

LIST OF ILLUSTRATIONS

Figure		Page
1	Schematic of test configuration	3
2	Microwave energy spectrum	9
3	Microwave chirping	10
4	Polarization of microwave pulses	11
5	S-band oscilloscope traces for various plasma densities	12
6	Magnitudes of peak emission power versus plasma density	13
7	Raggedness of microwave response	14

LIST OF TABLES

Table		Page
1	Microwave frequency bands	2
2	Microwave filter characteristics	4
3	Electron beam characteristics	5
4	Microwave power measurements, no plasma	7
5	Microwave receiver parameters	7

SECTION 1

TEST CONFIGURATION

The experimental volume consisted of a right-octagonal cylinder, constructed from half-inch thick Lexan, of 18-inch inside diameter and 24 inches in length. The end flanges of the chamber were fabricated from metal and connected to each other and ground. This construction allowed placement of the microwave receivers in the far field, outside the chamber, since the dielectric material is transparent to microwave radiation. The test chamber was evacuated to residual pressure in the range 10^{-5} to 10^{-4} Torr, using nitrogen to flush the ambient environment. During most of the test period the actual chamber pressure was not known because the pressure diagnostics were not operating reliably.

The microwave signal lines were terminated in an RF box located approximately 4 feet directly behind the experimental chamber. The EMP coupling to the signal lines was negligible. Instrumentation lines were contained in metal conduit all the way to the screen room. This was necessary as EMP coupling to the instrumentation lines was found to be severe without additional shielding. Signals were recorded on Tektronix 400-series oscilloscopes with frequency response of at least 150 MHz. Permanent records were made using photographic film. Due to the high-frequency oscillations of the signals and the generally poor writing quality of the recording instrumentation, 20-MHz filters were used.

A hot-filament, tungsten wire source was used to provide a steady-state plasma. Two generators, one at each end of the chamber, were capable of producing a plasma density of about 10^{10} electrons/cm³. The temperature of the plasma varied between 1 and 3 eV. Plasma density was reduced by lowering the filament supply current.

SECTION 2

DIAGNOSTIC EQUIPMENT

2.1 MICROWAVE

Measurements of the microwave emission were made with crystal detectors into a 7-channel microwave receiving system. The frequency channels and band designations are listed in Table 1. A schematic of the system is shown in Figure 1. Standard gain horn antennae were used to receive the microwave radiation. Each antenna was placed in the far field and directed radially to the axis of the electron beam, oriented so that the electric field plane was parallel to the electron beam. Except for the two highest frequency bands, each antenna was connected to a coaxial transformer through 1-1/3 meters of waveguide, then to the crystal detector through 2 meters of solid-shield, air-dielectric, coaxial cable. The X- and Ku-bands employed 3-1/3 meter lengths of waveguide all the way to the detector.

To eliminate out-of-band signal contamination, high- and low-pass filters were used. Signals outside the bandpass of the filters were attenuated by at least 55 dB. The coaxial high-pass filters were a redundant feature since waveguide naturally acts as a high-pass filter. However, there was not time to verify the high-pass filter characteristics of the actual waveguide. High-pass

Table 1. Microwave frequency bands.

Band	Frequency (GHz)
L	1.12 - 1.70
W	1.70 - 2.60
S	2.60 - 3.95
C	3.96 - 5.85
J	5.85 - 8.20
X	8.20 - 12.4
Ku	12.4 - 18.0

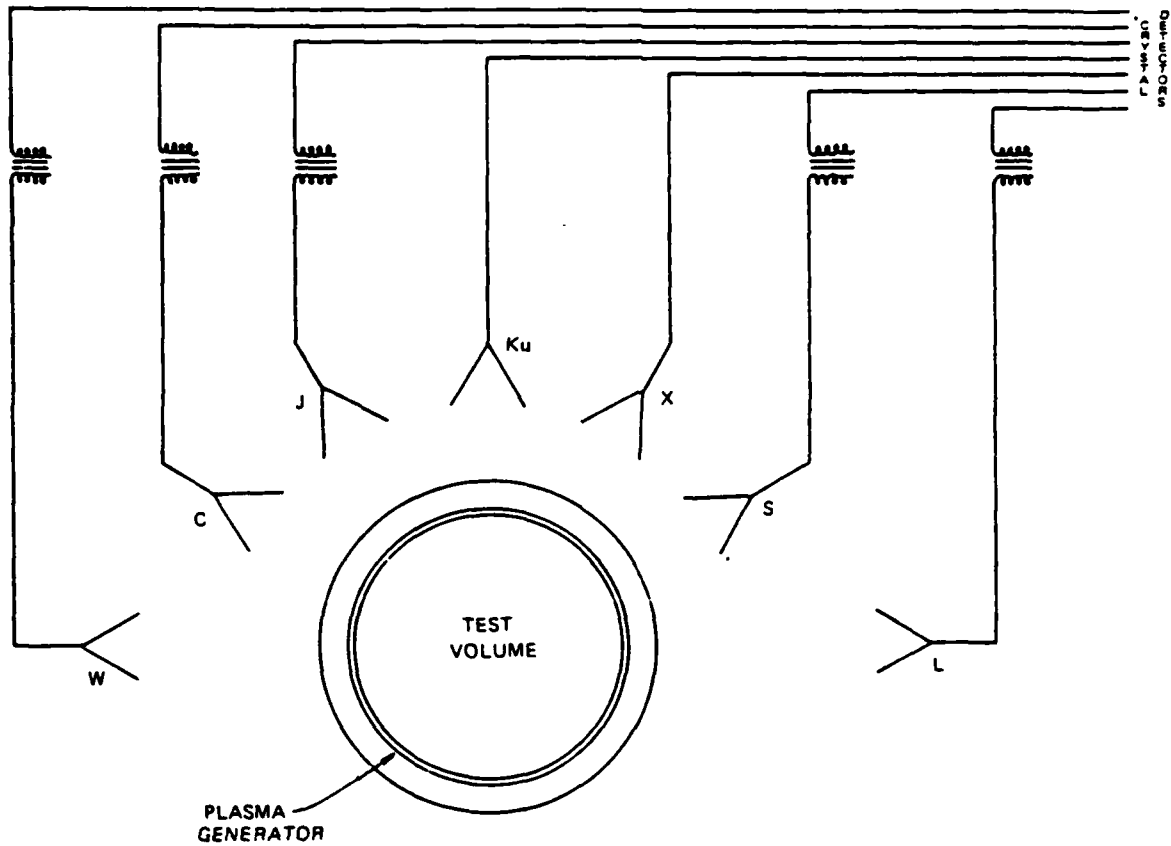


Figure 1. Schematic of test configuration.

filters were not used for the X- and Ku-bands since the waveguide lengths were more than sufficient to insure proper filtering. External filtering is listed in Table 2.

Crystal detectors are very sensitive to damage at relatively low power levels. Attenuation was used to reduce power levels well below the manufacturer's maximum input level. Fixed value, coaxial attenuators were used for bands L through J and variable waveguide attenuators were used for the X- and Ku-bands.

All of the microwave diagnostic hardware was bench-calibrated before use.

Table 2. Microwave filter characteristics.

Band	Natural Performance		External Filtering	
	-3 dB Bandpass (GHz)	Cutoff (GHz)	-25 dB (GHz)	-50 dB (GHz)
L	1.12 - 1.70	0.91	0.8 - 2.4	0.5 - 3.0
W	1.70 - 2.60	1.37	1.2 - 3.6	0.8 - 4.5
S	2.60 - 3.95	2.08	1.6 - 4.8	1.0 - 6.0
C	3.95 - 5.85	3.15	2.8 - 7.2	1.8 - 9.0
J	5.85 - 8.20	4.30	4.0 - 10.8	2.5 - 13.5
X	8.20 - 12.4	6.56		16.0
Ku	12.4 - 18.0	9.47		23.0

2.2 ELECTRON BEAM

The parameters characterizing the electron beam were measured by the facility operators. These included electron energy and current as a function of time. A direct measurement of the electron-beam energy was precluded early in the testing when the voltage probe was destroyed. A current sensor at the end of the diode chamber provided a measure of the total current entering our experimental chamber.

Current distribution within the experimental chamber was measured with current collectors of various diameters. Attempts at determining the magnetic fields within the chamber were made, but the signal-to-noise ratio was poor due to EMP coupling to the exposed signal lines.

2.3 AMBIENT PLASMA

The density and temperature of the plasma were estimated using data from a cylindrical Langmuir probe. The probe was fabricated from KSC ceramic-dielectric coaxial cable to minimize temperature effects. It was connected through a vacuum feedthrough, which allowed sampling of the plasma along the length of the chamber. Current versus applied voltage was recorded on an X-Y plotter.

SECTION 3

TEST MATRIX

A summary of the diode configurations used is given in Table 3. Initial operation was with an 18-inch-diameter diode using a cathode of graphite felt. The anode cathode gap was 1 cm, and the auxiliary control gap was 3 mm. This configuration produced an electron beam of about 100 keV peak and with an average current density of 2 A/cm². Next, the cathode diameter was reduced to 12 inches. The beam peak voltage rose to 140 keV, but the average current density remained essentially unchanged. The diode would not operate at smaller anode cathode gaps. This was most likely due to the filamentary nature of the graphite felt. Increasing the auxiliary gap produced a modest gain in current density. A graphite cathode was then used with a main gap of 7 mm and an auxiliary gap of 1.5 cm. This resulted in an electron current density of about 7 A/cm². Decreasing the gap to 3 mm produced no beam.

Table 3. Electron beam characteristics.

No.	Diode Configuration			Peak Energy (keV)	Injected Current Density (A/cm ²)
	Diameter (inches)	a-K (mm)	Auxiliary Gap (mm)		
I	18	10	3	100	2.2
II	12	10	3	140	2.1
III	12	10	5	---	3.4
IV	12	10	7	---	3.6
V	12	7	15	---	6.8

SECTION 4

TEST RESULTS

4.1 CALIBRATION MEASUREMENTS

Broadband microwave radiation was measured with no ambient plasma. The results were reproducible within the experimental error. The amplitude of the microwave power varied directly with external attenuator settings, verifying that microwave radiation was indeed being measured. Furthermore, placement of anechoic material between the source region and antenna eliminated the signal for that band. Covering the chamber with a layer of aluminum foil substantially reduced the microwave radiation.

As the current density increased, so did the microwave radiation emission. A summary of the microwave signals in the absence of plasma is given in Table 4. The microwave average power at the source was derived from converting the crystal detector voltage signal to power at the detector, using the individual crystal calibrations, correcting for external attenuation, compensating for loss in the signal line, and then using a form factor relating the effective area of the antenna to the source area at the receiver. The various parameters used are shown in Table 5.

4.2 PLASMA MEASUREMENTS

During the final 4-7 September period of testing a limited number of microwave measurements with the ambient plasma were performed (31 shots and 132 scope traces were made with the plasma). Introduction of the plasma increased the complexity of the experiment and generally each shot was a unique event. As such, these preliminary measurements are little more than anecdotal. Nevertheless, when combined with theoretical work and other experimental results, they lead to some provocative speculation. The upcoming series of experiments will allow statements that are more definitive.

Table 4. Microwave power measurements, no plasma.

Band	Power (average over pulse width) (kW/GHz \pm 50% rms)				
	I	II	III	IV	V
L	300	80	40	31	41
W	960	2,500	670	840	760
S	2,700	2,400	720	1,200	1,000
C	28	35	1,900	3,500	3,200
J	7	9	6	16	40
X	2	2	22	15	15
Ku	0.7	0.9	5	9	3
L-Ku	280	330	320	550	490
Total (kW)	4,700	5,600	5,400	9,300	8,300
τ (ns)	32	33	38	26	33
Energy (J)	0.15	0.18	0.21	0.24	0.27

Table 5. Microwave receiver parameters.

Band	Antenna		Area (cm ²)	Source Distance (cm)	Form Factor
	Line Loss (dB)	Gain (dB)			
L	1.5	15.5	1,405	211	398
W	1.5	15.5	602	110	253
S	1.5	16.6	328	89	303
C	1.7	16.5	146	102	895
J	1.9	22	243	81	339
X	2.2	22	117	79	670
Ku	2.6	24	84	91	1,240

For low beam-plasma density ratio (less than 0.1), the plasma has sufficient conductivity to short out the beam current. The beam is observed to transport across the chamber, inducing small fields and negligible microwave emission. This is consistent with the theoretical understanding of the system.

For a stronger beam, the measurement of the microwave radiation revealed a marked difference. As the beam-plasma ratio approached unity, broadband microwave radiation was observed. Figure 2 shows a plot of the energy emitted versus frequency for our system. This is for a very intense beam ($\sim 10 \text{ A/cm}^2$) and most of the energy is in the C-band (4-6 GHz). This emission peak is far above the ambient plasma frequency, which is at most about 1 GHz.

This measured microwave emission occurs during the entire beam pulse duration. The lowest frequency peaks first and then the higher bands peak sequentially infrequency. Figure 3 shows this result quite clearly. This is a plot of the channel frequency versus time of peak power for a low plasma density ($10^9 \text{ electrons/cm}^3$). The L-band emission comes on simultaneously with the beam. The Ku-band is excited just before the end of the beam pulse. The chirping proceeds exponentially in time. It is far too fast for any avalanche process at an air density of 0.1 micron. The chirping has been observed on other experiments at Physics International and University of California--Irvine, and is believed to be related to the diode voltage and, thus, the distribution of emitted electrons.

The scope traces themselves also provide evidence as to the nature of the production mechanisms involved. Our microwave measurements with the ambient plasma are often double-humped. The bimodal response was checked by changing the equipment and analyzing the time difference. It indicates that there are probably two different mechanisms producing the microwaves. The possibility is much more probable based on the results shown in Figure 4. The right-hand trace has the pickup antenna rotated 90° to pick up fields in the azimuthal (instead of axial) direction. All other conditions remained the same. A dramatic difference in the relative size of the two pulses is observed. Both pulses are somewhat polarized since both their magnitudes are reduced. The first pulse is only modestly polarized since its magnitude is only reduced by about 30 percent. The second pulse is strongly polarized; its magnitude is reduced by more than 90 percent.

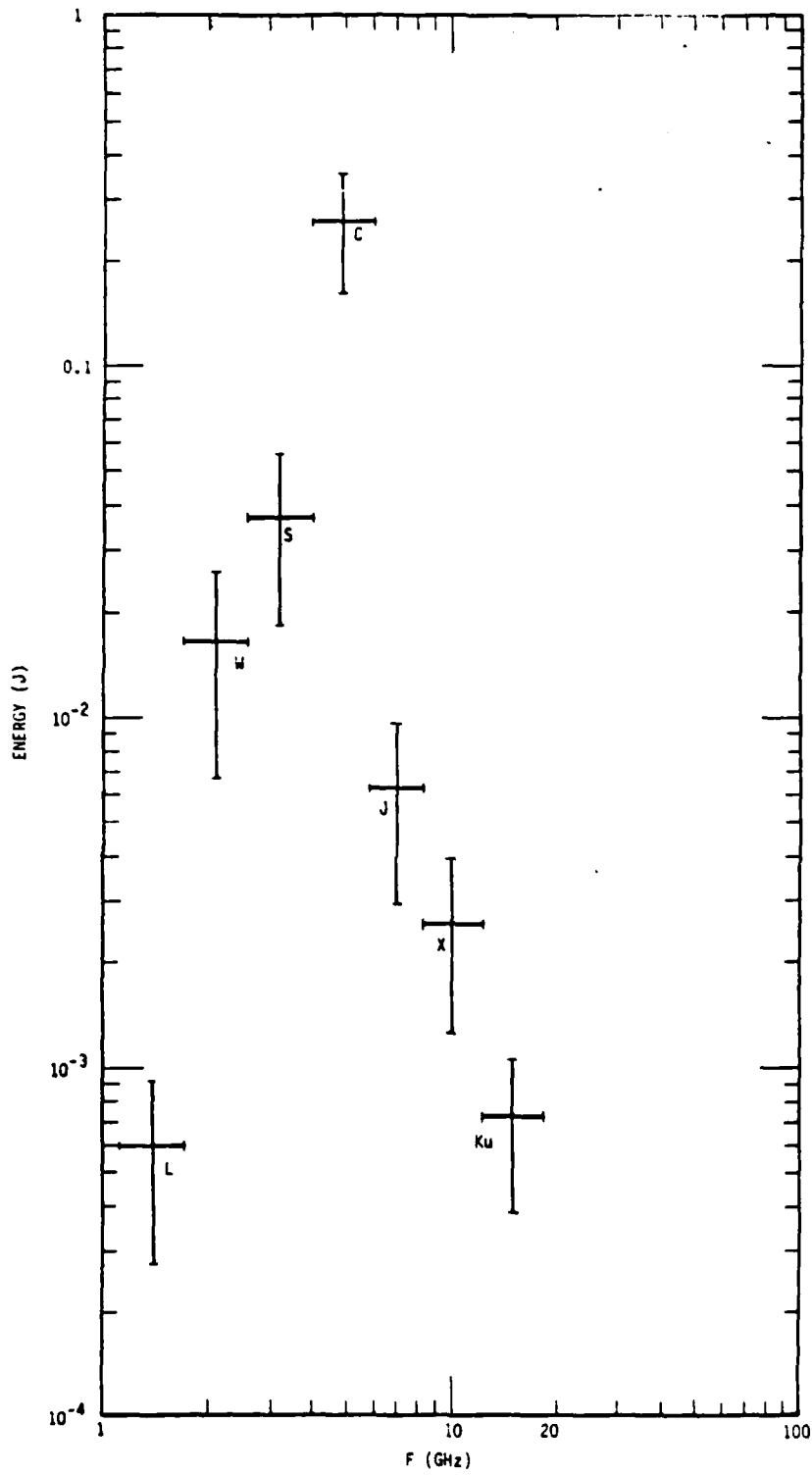


Figure 2. Microwave energy spectrum.

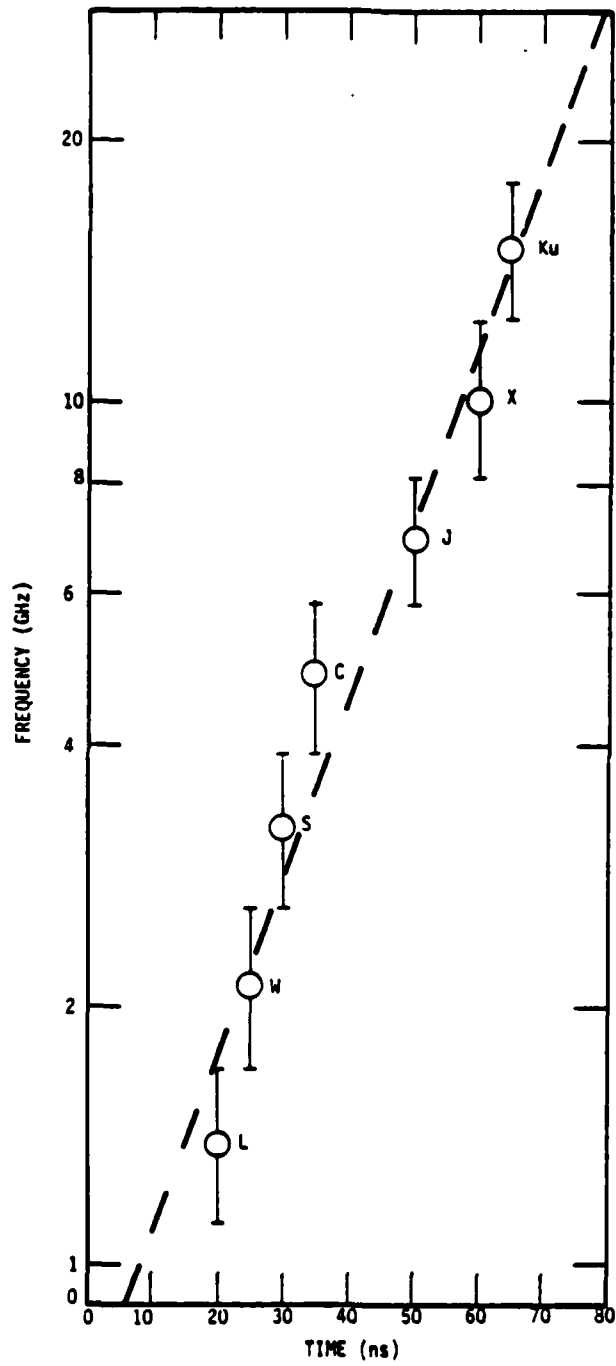
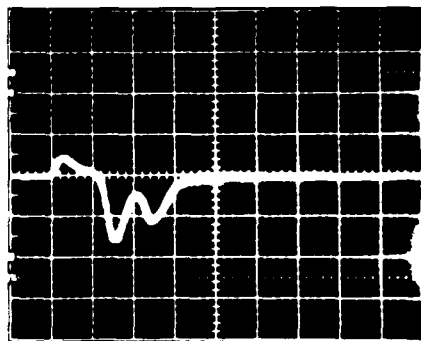
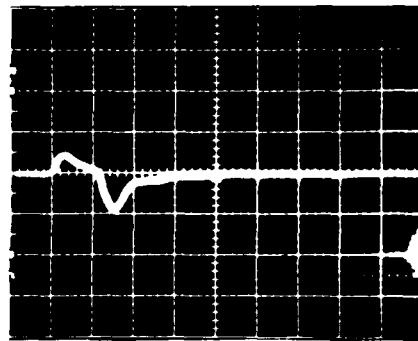


Figure 3. Microwave chirping.



ANTENNA PARALLEL
TO CHAMBER AXIS



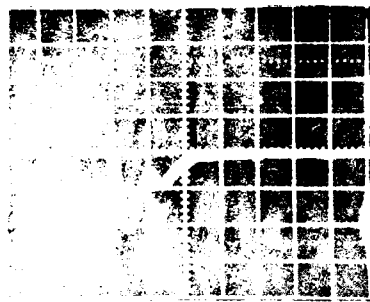
ANTENNA PERPENDICULAR
TO CHAMBER AXIS

Figure 4. Polarization of microwave pulses.

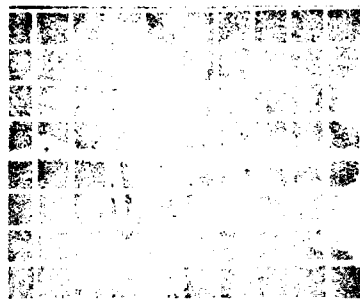
The behavior of the two pulses is further analyzed in the series of scope traces shown in Figure 5. The effect of changing the plasma density on the relative magnitude of the two pulses is shown. As in Figure 4, these are data from the S-band horn. Again, the attenuators and all experimental details except for the plasma discharge current are kept constant from shot to shot. When there is a tenuous plasma, the first peak is definitely dominant. As the plasma density is increased, the relative amplitude of the second pulse grows. It becomes larger than the first. With sufficient plasma, the emission in the second pulse is also quenched. The relative magnitude of the pulses is summarized in Figure 6.

We believe the first microwave pulse is related to transient fields and reflexing phenomena in the surface of the beam-electron distribution. The second pulse is related to plasma emission phenomena in the volume of the beam.

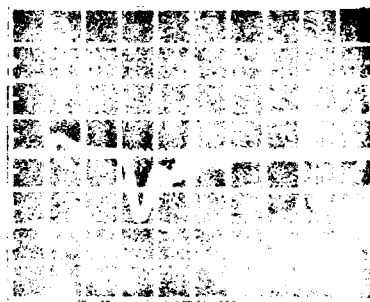
Another quality of the scope traces that is very distinct is their roughness. In Figure 7, a couple of scope traces with and without the 20-MHz filter are shown. The general trend of the signals (i.e., with the filter) are repeatable, while the finer detail is not. These preliminary experiments have focused on the average trend and generally the 20-MHz scope filter was applied. The unfiltered signals have structure that approaches the limit of the oscilloscopes and crystal detectors so the ultimate raggedness of the emission may not be revealed. The frequencies being measured are only a few gigahertz, which means that the structure we are observing may be intrinsically related to the fundamental process producing the EM radiation.



VACUUM



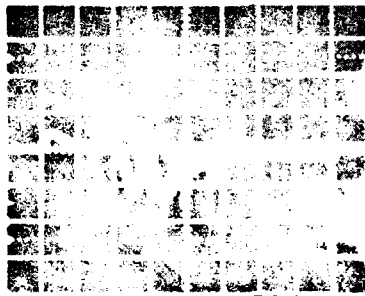
7×10^8



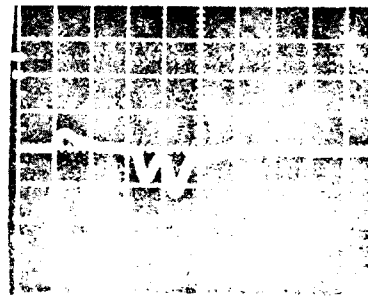
10^9



3×10^9



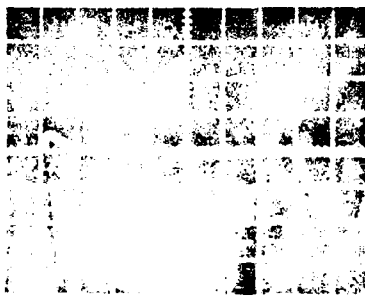
5×10^9



7×10^9



9×10^9



10^{10}



2×10^{10}

(electrons/cm³)

Figure 5. S-band oscilloscope traces for various plasma densities.

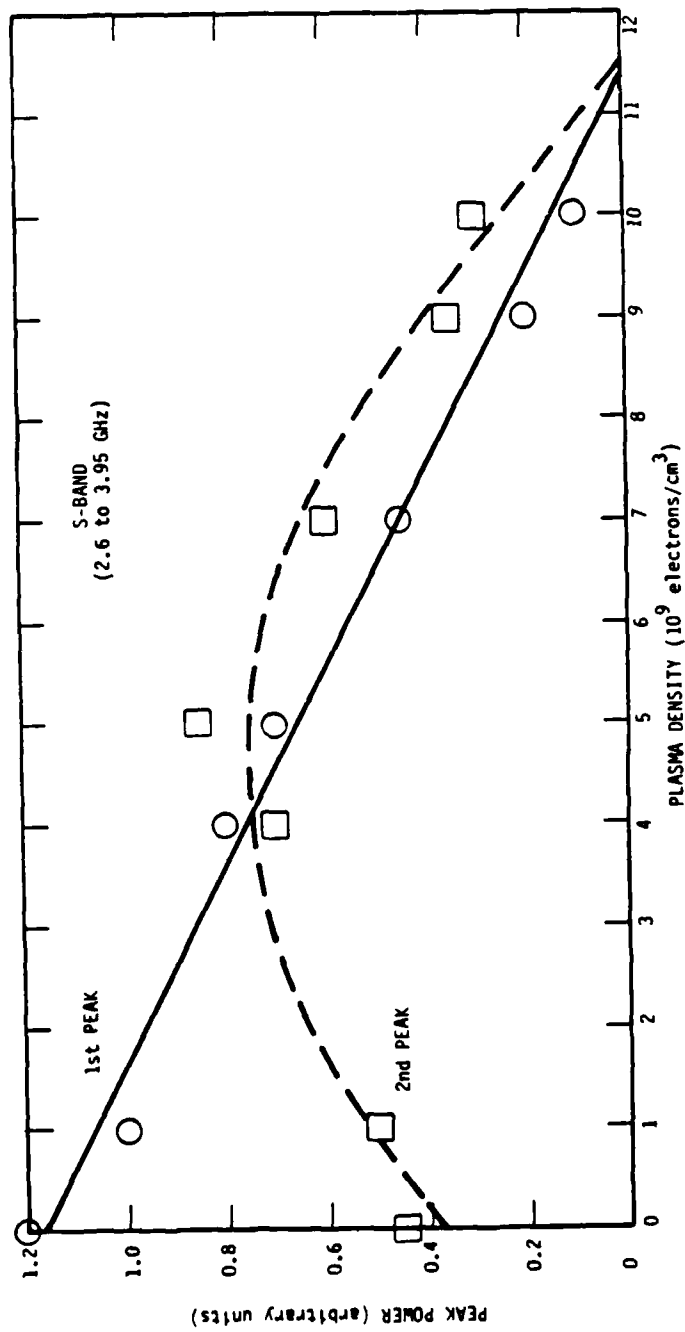


Figure 6. Magnitudes of peak emission power versus plasma density (see Figure 5).

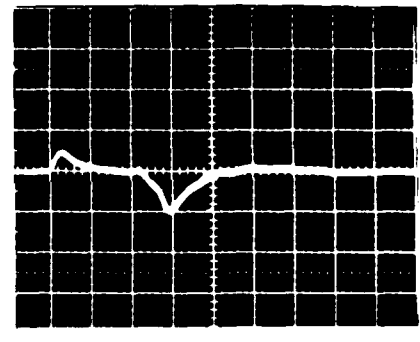
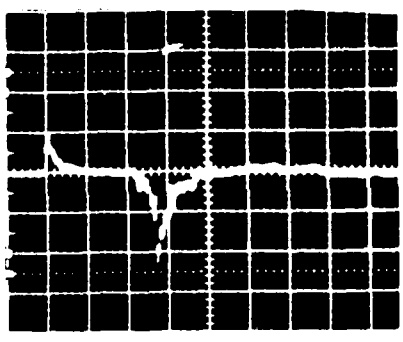
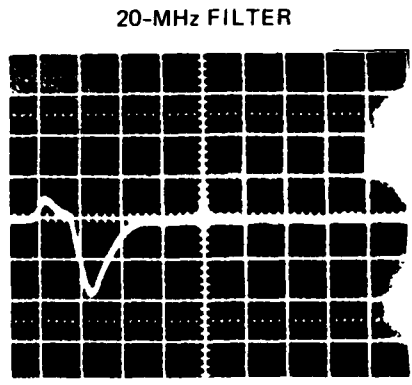
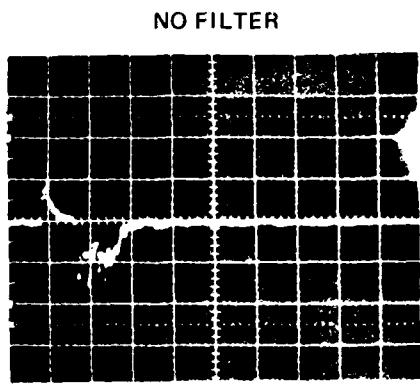


Figure 7. Raggedness of microwave response.

SECTION 5

RECOMMENDATIONS

This initial test series has revealed several areas where improvements are indicated to achieve the program objectives. The areas affected include planning, diagnostics, sources, facility operation, and data acquisition/reduction.

Now that the basic techniques for microwave measurements are understood and the operation of the simulator has been observed, better planning can be accomplished. The understanding will be that the MBS will operate as designed and the limitations of the plasma generator(s) will be known.

The electron beam and plasma diagnostics require improvement and/or additions. The present current collector needs to be replaced with a segmented collector to provide uniformity information without taking numerous shots. An electron spectrometer, available from Chomerics at no charge, would provide valuable information. However, hardware changes would be required and some time would be involved in the data collection. The magnetic field probes fabricated for the initial test series need to have shielded signal lines; otherwise they work fine. A better design is needed for the Langmuir probe, allowing greater freedom of movement without disturbing the vacuum integrity of the test volume, and the ability to retract the probe during a shot. It may prove beneficial to use a microwave interferometer.

A pulsed plasma source is needed to produce densities greater than 10^{12} electrons/cm³. The titanium hydride generator used by Kato would serve the purpose; multiple sources would be required to produce a homogeneous plasma. Note that a microwave interferometer is required for this type of generator. An alternative steady-state source that may approach 10^{12} electrons/cm³ is the lanthanum hexaboride paste filament system.

Several improvements to the electron generator are required. The generator has potential to produce several hundred kiloamperes short circuit. Operating with a diode load, space charge limits densities to about 60 A/cm^2 , or 44 kA

peak, for a 30-cm diameter beam. Higher densities may be realized for smaller beam diameters. During our experiments the maximum current observed was only 10 kA without space-charge neutralization. Secondly, although the use of graphite felt for a cathode was convenient, it precluded using small diode gaps and tended to explode easily, requiring machine downtime to change. The anode is too large, making it a time-consuming process to change. Better control over the gap spacing, i.e., diode planarity, is needed. Reliable machine diagnostic monitors are necessary. The anode needs to be moved closer to the test chamber entrance.

The acquisition and reduction of the vast quantity of data needs to be automated. There is a computer system at Physics International that we need to use, provided it can turn around fast. We need to see our data within minutes.

DISTRIBUTION LIST

DEPARTMENT OF DEFENSE

Defense Intell Agency
ATTN: RTS-2B

Defense Nuclear Agency
2 cys ATTN: RAEV
4 cys ATTN: STTI-CA

Defense Tech Info Ctr
2 cys ATTN: UD

Field Command, DNA, Det 2
Lawrence Livermore National Lab
ATTN: FC-1

Field Command, Defense Nuclear Agency
ATTN: FCPR
ATTN: FCIT, W. Summa
ATTN: FCTXE

Joint Strat Tgt Planning Staff
ATTN: JLAA
ATTN: JLK, DNA Rep
ATTN: JKLS
ATTN: JPTM

DEPARTMENT OF THE ARMY

BMD Advanced Technology Ctr
ATTN: ATC-0

BMD Systems Command
ATTN: BDMSC-H

Harry Diamond Laboratories
ATTN: DELHD-NW-RH, R. Gilbert, 22800
ATTN: DELHD-TA-L, 81100, Tech Lib

USA Missile Command
ATTN: Doc Section

DEPARTMENT OF THE NAVY

Naval Research Laboratory
ATTN: Code 4720, J. Davis
ATTN: Code 6610, J. Ritter
ATTN: Code 6701
ATTN: Code 6707, K. Whitney

Naval Surface Weapons Center
ATTN: Code F31

Space & Naval Warfare Systems Cmd
ATTN: PME-106-1

Strategic Systems Programs, PM-1
ATTN: NSP

DEPARTMENT OF THE AIR FORCE

Air Force Geophysics Laboratory
ATTN: PH, C. Pike

Air Force Operational Test & Eval Ctr
ATTN: UA1, Capt Lutz

DEPARTMENT OF THE AIR FORCE (Continued)

Air Force Space Technology Ctr
ATTN: A. Gunther

Air Force Weapons Laboratory
ATTN: NT
ATTN: NTN
ATTN: SUL
2 cys ATTN: NTC

Ballistic Missile Office, DAA
ATTN: ENMG
ATTN: ENSN

Rome Air Development Center
ATTN: ESR/ET, E. Burke, M/S 64

Space Command
ATTN: XPM

Strategic Air Command
ATTN: NRI/STINFO
ATTN: XPFS

DEPARTMENT OF ENERGY

University of California
Lawrence Livermore National Lab
ATTN: Tech Info Dept Lib

Los Alamos National Laboratory
ATTN: MS P364, Reports Lib

Sandia National Laboratories
ATTN: T. Dellin

Sandia National Laboratories
ATTN: Org 1232, W. Beezhold
ATTN: Org 9336, D. Allen
ATTN: Tech Lib, 3141

OTHER GOVERNMENT AGENCIES

National Oceanic & Atmospheric Admin
ATTN: F. Fehsenfeld

NASA, Lewis Research Center
ATTN: C. Purvis
ATTN: Library

DEPARTMENT OF DEFENSE CONTRACTORS

Advanced Research & Applications Corp
ATTN: R. Armistead

Aerojet Electro-Systems Co
ATTN: SV/8711/70

Aerospace Corp
ATTN: D. Schmunk
ATTN: J. Reinheimer
ATTN: Library
ATTN: P. Hansen
ATTN: V. Josephson

DEPARTMENT OF DEFENSE CONTRACTORS (Continued)

AVCO Systems Division
ATTN: Library, AB30

BDM Corp
ATTN: D. Harmony

Beers Associates, Inc
ATTN: B. Beers

Berkeley Rsch Associates, Inc
ATTN: E. Alcaraz

Boeing Co
ATTN: MS-2R-00, J. Arimura

Computer Sciences Corp
ATTN: A. Schiff

Dikewood Corp
ATTN: Tech Lib

Dikewood Corp
ATTN: K. Lee

EC&G Wash Analytical Svcs Ctr, Inc
ATTN: Library

Electro-Magnetic Applications, Inc
ATTN: E. Mann
ATTN: W. Zimmerman

General Electric Co
ATTN: D. Tasca
ATTN: H. O'Donnell
ATTN: J. Peden

General Research Corp
ATTN: A. Hunt

Hughes Aircraft Co
ATTN: Tech Lib

Hughes Aircraft Intl Svc Co
ATTN: A. Narevsky, S32/C332
ATTN: L. Darda
ATTN: N. Milin

IRT Corp
ATTN: B. Williams
ATTN: Library
ATTN: N. Rudie

IRT Corp
ATTN: J. Klebers

JAYCOR
ATTN: D. Higgins

JAYCOR
ATTN: E. Wenaas
ATTN: Library
ATTN: R. Stahl

JAYCOR
ATTN: R. Sullivan

JAYCOR
ATTN: R. Poll

DEPARTMENT OF DEFENSE CONTRACTORS (Continued)

JAYCOR
ATTN: M. Bell

Johns Hopkins University
ATTN: P. Partridge

Kaman Sciences Corp
ATTN: D. Osborn
ATTN: Library
ATTN: N. Beauchamp
ATTN: W. Rich
2 cys ATTN: S. Face
2 cys ATTN: W. Hobbs
2 cys ATTN: E. Cozart
2 cys ATTN: T. Tumolillo

Kaman Sciences Corp
ATTN: E. Conrad

Kaman Tempo
ATTN: DASIAC
ATTN: W. McNamara

Kaman Tempo
ATTN: DASIAC
ATTN: R. Mahoney

Lockheed Georgia Co
ATTN: Dept 662, E. Harris

Lockheed Missiles & Space Co, Inc
ATTN: L. Chase

McDonnell Douglas Corp
ATTN: R. Kloster

McDonnell Douglas Corp
ATTN: S. Schneider

Mission Research Corp
ATTN: C. Longmire
ATTN: M. Scheibe
ATTN: R. Stettner

Mission Research Corp
ATTN: W. Ware

Mission Research Corp, San Diego
ATTN: Library

Pacific-Sierra Research Corp
ATTN: H. Brode, Chairman SAGE
ATTN: I. Schlessinger

R&D Associates
ATTN: C. Knowles
ATTN: S. Siegel
ATTN: Tech Info Ctr

Rand Corp
ATTN: P. Davis

Rand Corp
ATTN: B. Bennett

Rockwell International Corp
ATTN: Library

DEPARTMENT OF DEFENSE CONTRACTORS (Continued)

Rockwell International Corp
ATTN: TIC, AJ01

S-CUBED
ATTN: A. Wilson
ATTN: Library

SRI International
ATTN: Library

DEPARTMENT OF DEFENSE CONTRACTORS (Continued)

Science Applications Intl Corp
ATTN: J. Tigner
ATTN: W. Chadsey

TRW Electronics & Defense Sector
ATTN: D. Clement
ATTN: R. Kingsland
ATTN: Tech Info Ctr

END
FILMED

5-86

DTIC